Recursive Model-agnostic Inverse Dynamics of Serial Soft-Rigid Robots: Supplementary Material

International Journal of Robotics Research
XX(X):1–5

DOI: 10.1177/ToBeAssigned
www.sagepub.com/
SAGE

Pietro Pustina[1, 2], Cosimo Della Santina[2, 3] and Alessandro De Luca[1]

1 Extra Numerical Results

This document presents additional simulation results with the inverse dynamics algorithms presented in Pustina et al. (2025).

Note: All the numerical results are obtained with the same inverse dynamics algorithm. The MATLAB code used for the simulations can be accessed at the following link: `https://github.com/piepustina/Jelly`.

1.1 Simulation 4: PCC with variable radius

Consider a planar soft robot actuated with three pairs of antagonistic pneumatic chambers. In the following, we show that the generic kinematics function used in Pustina et al. (2025) allows us to easily model the effects of the chambers on the dynamics by introducing additional DoF for the radius change. To the best of our knowledge, this is the first time that such class of models is presented and simulated, and thus constitutes an additional contribution of our work.

Specifically, we model the kinematics by using a combination of strain and radial configuration variables. The strain configuration encodes the pose of the robot backbone, while the radial variables model the shape alterations along the robot section. The continuum is discretized into three bodies with cylindrical shape in the stress free configuration, having each rest length $L_{0_i} = 0.2$ [m], radius $R_{0_i} = 0.02$ [m] and mass density $\rho_i = 1062$ $[\mathrm{kg\,m^{-3}}]; i = 1, 2$. The material visco-elastic parameters are $C_i = 0.501[\mathrm{MPa}]$ and $\eta_i = 0.1$ [s]. The base is rotated so that in the straight configuration the robot is aligned with the gravitational field and points downwards. Each pneumatic chamber has a uniform distance $d_{c,i} = 0.004$ [m] from the body walls.

Each body $\mathcal{B}_i$ has in total four DoF. The first two model the curvature and elongation strains under the PCC hypothesis, i.e.,

$$\begin{pmatrix} \kappa_i(\boldsymbol{q}_i) \\ \delta L_i(\boldsymbol{q}_i) \end{pmatrix} = \frac{1}{L_{0_i}} \begin{pmatrix} 1 & 0 & 0 & 0 \\ 0 & 1 & 0 & 0 \end{pmatrix} \boldsymbol{q}_i + \begin{pmatrix} 0 \\ 1 \end{pmatrix}.$$

The remaining two configuration variables describe the change in radius R_i, namely

$$R_i(s_i, \phi_i, , \boldsymbol{q}_i) = R_{0_i} + \delta R_i(s_i, \phi_i, \boldsymbol{q}_i),$$

where

$$\delta R_i = \begin{cases} \begin{pmatrix} 0 & 0 & b(s_i, \phi_i) & 0 \end{pmatrix} \boldsymbol{q}_i, & \begin{array}{l} s_i \in [0, L_{0,i}], \\ \phi_i \in [0, \pi); \end{array} \\ \begin{pmatrix} 0 & 0 & 0 & b(s_i, \phi_i - \pi) \end{pmatrix} \boldsymbol{q}_i, & \begin{array}{l} \phi_i \in [0, L_{0,i}], \\ \phi_i \in [\pi, 2\pi). \end{array} \end{cases},$$

models the radius change from R_{0_i}. The angular variable ϕ_i is used to locate for each cross section the pneumatic chamber. To model the functional dependence of δR_i on the material coordinates, in this case s_i, ϕ_i and the radius R_{0_i} in the stress free-configuration, we use the multivariate bump function

$$b(s_i, \phi_i) = e^{-\frac{L_{0_i}}{\frac{L_{0_i}^2}{4} - (s_i - \frac{L_{0_i}}{2})^2}} e^{-\frac{1}{\frac{\pi^2}{4} - (\phi_i - \frac{\pi}{2})^2}}.$$

This choice is motivated by empirical observation of pneumatically actuated soft robots, whose chamber deformation is usually larger at the middle of body.

The actuation generalized force $\boldsymbol{\nu}_i(\boldsymbol{q}_i, \boldsymbol{u}_i)$ of $\mathcal{B}_i$ is modeled using the principle of virtual works leading to

$$\boldsymbol{\nu}_i(\boldsymbol{q}_i, \boldsymbol{u}_i) = \nabla_{\boldsymbol{q}_i} \boldsymbol{V}_i(\boldsymbol{q}_i) \boldsymbol{u}_i, \tag{1}$$

where the vector $\boldsymbol{V}_i(\boldsymbol{q}_i) = (V_{i,1}(\boldsymbol{q}_i) \;\; V_{i,2}(\boldsymbol{q}_i))^T$ collects the volume of the two pneumatic chambers in the current configuration and $\boldsymbol{u}_i = (u_{i,1} \;\; u_{i,2})^T$ is the difference in chamber pressure with respect to the atmospheric pressure. The robot starts at rest from the stress free configuration $\boldsymbol{q}_0 = \boldsymbol{0}_{12}$ and the dynamics is excited with a constant input equal to

$$\boldsymbol{u} = \begin{pmatrix} 2 & 0 & 0 & 2 & 1 & 0.4 \end{pmatrix}^T \text{ [MPa]}.$$

The volume integrals appearing in the ID algorithms and (1) are approximated using a Gaussian quadrature rule in spherical coordinates. Fig. 1 reports the time evolution of the configuration variables, divided into strain and radial variables, and a stroboscopic plot of the robot motion in its workspace.

1.2 Simulation 5: PGC in free evolution

Consider a tentacle-like soft robotic arm of two bodies with conical shape. The first body has base and tip radius equal

[1] Department of Computer, Control and Management Engineering, Sapienza University of Rome, Rome, IT.
[2] Department of Cognitive Robotics, Delft University of Technology, Delft, NL.
[3] Institute of Robotics and Mechatronics, German Aerospace Center (DLR), Oberpfaffenhofen, GER.

Corresponding author:
Pietro Pustina, pietro.pustina@uniroma1.it

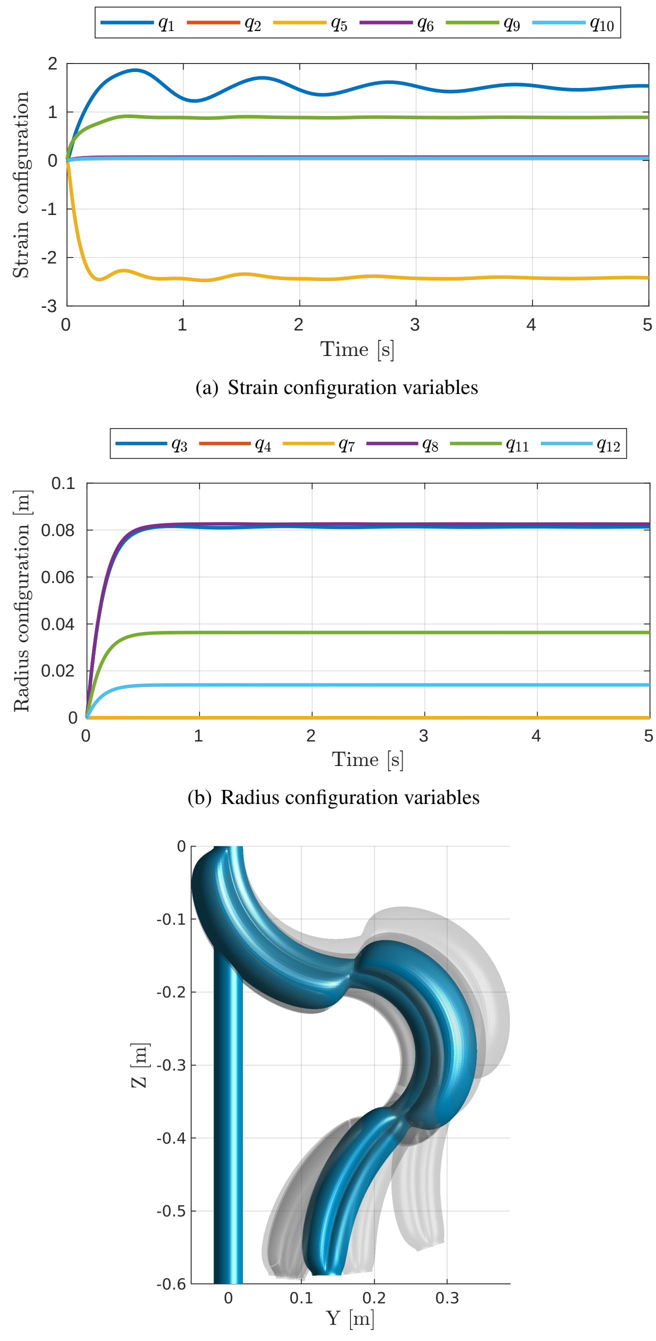

(a) Strain configuration variables

(b) Radius configuration variables

(c) Stroboscopic plot

Figure 1. Simulation 4: PCC with variable radius. Time evolution of the (a) strain (in [rad] and [m]) and (b) radial configuration variables, and (c) stroboscopic plot of motion. The robot consists of three bodies with variable radius and is actuated through six pressure chambers. In (c), the initial and final configurations are depicted in blue, while the transient motion in light gray.

to $R_{\text{base}_1} = 0.01$ [m] and $R_{\text{tip}_1} = 0.005$ [m], respectively, while the second $R_{\text{base}_2} = 0.005$ [m] and $R_{\text{tip}_2} = 0.002$ [m]. The rest length and mass density are $L_{0_i} = 0.2$ [m] and $\rho_i = 1070\,[\text{kg}/\text{m}^3]$, respectively. The elastic parameter is $C_i = 0.111$ [GPa], while the material viscosity $\eta_i = 0.01$ [s]; $i = 1, 2$. The kinematics is computed using the Geometric Variable Strain approach of Renda et al. (2020). Inspired by Wang et al. (2022), we model the strain using a Piecewise Gaussian Curvature (PGC) basis with elongation, defined as follows

$$\begin{pmatrix} \kappa_{x,i} \\ \kappa_{y,i} \\ \delta L_i \end{pmatrix} = \boldsymbol{\Phi}_i(s_i)\boldsymbol{q}_i + \begin{pmatrix} 0 \\ 0 \\ 1 \end{pmatrix},$$

where

$$\boldsymbol{\Phi}_i(s_i) = \frac{1}{L_{0_i}} \begin{pmatrix} 0 & 0 & -1 & -e^{-(s_i - L_{0_i}/2)^2} & 0 \\ 1 & e^{-(s_i - L_{0_i}/2)^2} & 0 & 0 & 0 \\ 0 & 0 & 0 & 0 & 1 \end{pmatrix},$$

$s_i \in [0, L_{0_i}]$ and $\boldsymbol{q}_i \in \mathbb{R}^5$. The robot starts at rest from the initial configuration

$$\boldsymbol{q}_0 = \begin{pmatrix} 0.3 & 1 & 0 & 1 & 0.1 & -1 & 0 & 0.1 & 2 & 0 \end{pmatrix}^T,$$

and the base is rotated so that in the stress-free configuration the arm is aligned with the gravitational field with the tip pointing upwards. The results of the simulation are shown in Fig. 2. After a transient of approximately 5 [s], the arm reaches a steady-state position consistent with the direction of the gravitational force.

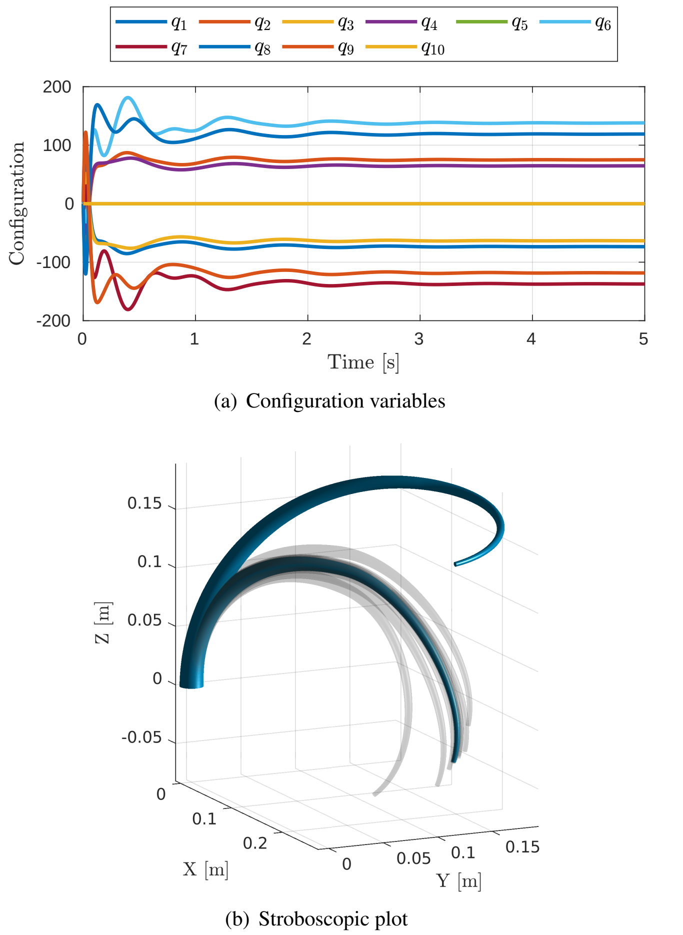

(a) Configuration variables

(b) Stroboscopic plot

Figure 2. Simulation 5: PGC in free evolution. Time evolution of the (a) configuration variables (in [rad] and [m]) and (b) stroboscopic plot of a slender continuum soft robot modeled with a Gaussian model of the strain. In (b), the initial and final configurations are depicted in blue, while intermediate configurations in light gray.

1.3 Simulation 6: PCC in free evolution

Consider a soft robot moving in free evolution under gravity. The arm consists of two slender silicone bodies with a cylindrical shape. The base is rotated so that in the reference (straight) configuration the robot extends along the Y axis, with the gravitational force acting in the Z direction. We assume that a PCC model can approximate the motion of each body. Thus, the configuration space of $\mathcal{B}_i$ has dimension three and $\boldsymbol{q}_{\mathcal{B}_i} = \boldsymbol{q}_i = (\kappa_{x,i}\ \kappa_{y,i}\ \delta L_i)^T \in \mathbb{R}^3$; $i = 1, 2$, where $\kappa_{x,i}$ and $\kappa_{y,i}$ represent the curvature along x and y, respectively, and δL_i is the rod elongation. The mass density is $\rho_i = 1070\,[\mathrm{kg/m^3}]$ and uniformly distributed along the body, whose radius is $R_i = 0.01\,[\mathrm{m}]$ and rest length $L_{0_i} = 0.3\,[\mathrm{m}]$. The stress parameters are $C_i = 0.555\,[\mathrm{GPa}]$ and $\eta_i = 0.333\,[\mathrm{s}]$. The robot starts at rest from the initial configuration

$$\boldsymbol{q}_0 = \begin{pmatrix} 1.5 & 1 & 0 & 1 & -1 & 0.1 \end{pmatrix}^T .$$

Fig. 3 reports the time evolution of the configuration variables and a stroboscopic motion plot.

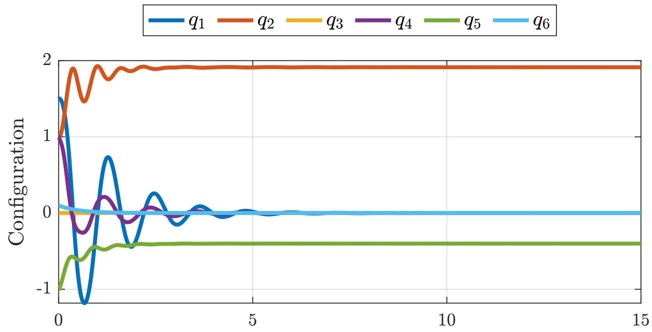

(a) Configuration variables

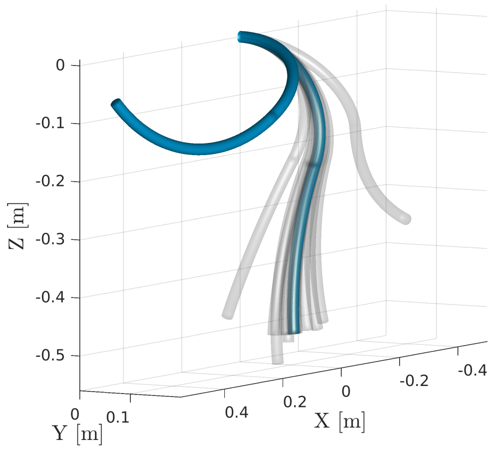

(b) Stroboscopic plot

Figure 3. Simulation 6: PCC in free evolution. Time evolution of the (a) configuration variables (in $[\mathrm{rad}]$ and $[\mathrm{m}]$) and (b) stroboscopic plot of the robot motion. The arm consists of two bodies modeled under the PCC hypothesis and moves in free evolution under gravity.

1.4 Simulation 7: PAC in free evolution

Consider the same soft robot of Section 1.3, but with a piecewise affine curvature (PAC) model, i.e.,

$$\begin{pmatrix} \kappa_{x,i} \\ \kappa_{y,i} \end{pmatrix} = \frac{1}{L_{0_i}} \begin{pmatrix} 0 & 0 & -1 & -\frac{s_i}{L_{0_i}} \\ 1 & \frac{s_i}{L_{0_i}} & 0 & 0 \end{pmatrix} \begin{pmatrix} q_{1,i} \\ q_{2,i} \\ q_{3,i} \\ q_{4,i} \end{pmatrix},$$

$s_i \in [0, L_{0_i}]$. We initialize the affine components to zero to start from the exact spatial configuration of Simulation 6. The outcomes of this simulation are depicted in Fig. 4. The steady-state configuration is different to the previous. However, as expected, the strain attains similar values at the tip of the two segments.

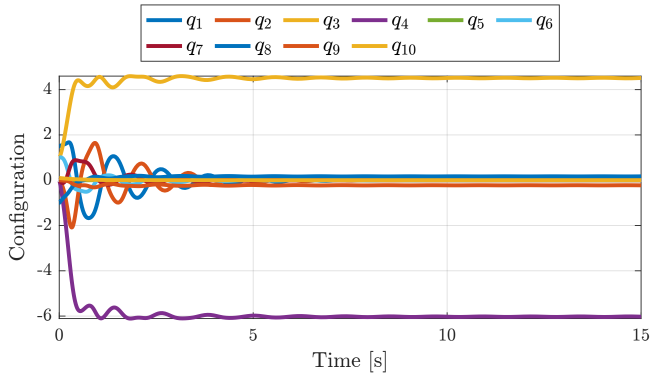

(a) Configuration variables

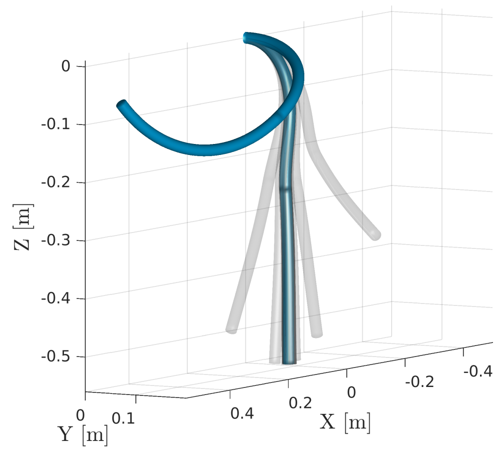

(b) Stroboscopic plot

Figure 4. Simulation 7: PAC in free evolution. Time evolution of the (a) configuration variables (in $[\mathrm{rad}]$ and $[\mathrm{m}]$) and (b) stroboscopic plot of a soft robot with the same physical parameters of the robot in Simulation 6 but with an affine model for the curvature strains.

1.5 Simulation 8: PCS in free evolution

We now assume that the robot takes configurations where all the strains are non-negligible and well approximated by a piecewise constant strain (PCS) model (Renda et al. 2018). Consequently, the configuration of each body is a six-dimensional vector containing the strains, constant in space but variable in time. The initial configuration is

$$\boldsymbol{q}_0 = \begin{pmatrix} 1.5 & 1 & 0.2 & 0.02 & 0 & 0 & 1 & -1 & -0.1 & 0 & -0.01 & 0.1 \end{pmatrix}^T,$$

with zero velocity. In Fig. 5, we present the time evolution of the configuration variables and the robot motion. The steady-state value of the curvature variables and elongations is consistent with those observed in Simulation 6.

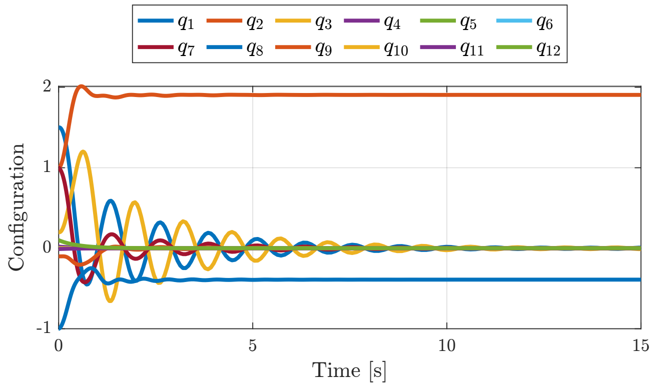

(a) Configuration variables

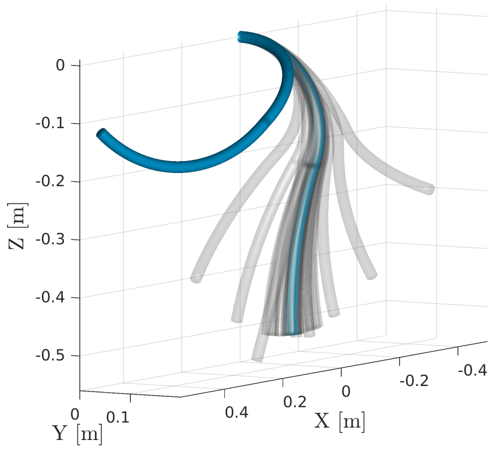

(b) Stroboscopic plot

Figure 5. Simulation 8: PCS in free evolution. Time evolution of the (a) configuration variables (in [rad] and [m]) and (b) stroboscopic plot for a soft robot with same physical parameters of the soft arm in Simulation 6. The configuration space is approximated adopting a PCS model of the strains.

1.6 Simulation 9: UR10 with PCC body

Consider a Universal Robots UR10 collaborative manipulator carrying a passive PCC cylinder of silicone on its tip. The latter has rest length $L_0 = 0.8$ [m], radius $R = 0.02$ [m], mass density $\rho = 1070\,[\mathrm{kg/m^3}]$, elastic coefficient $C = 8$ [GPa] and viscous parameter $\eta = 0.054$ [s]. The task is to control the robot joints to the reference trajectory

$$\boldsymbol{q}_{a_d}(t) = \cos(t)\mathbf{1}_6 \text{ [rad]}.$$

Partial feedback linearization (PFBL) on the collocated variables is used to fulfill the task. The control law is given by

$$\begin{aligned}\boldsymbol{\nu}_a = &(\boldsymbol{M}_{aa} - \boldsymbol{M}_{au}\boldsymbol{M}_{uu}^{-1}\boldsymbol{M}_{au}^T) \\ &\cdot [\ddot{\boldsymbol{q}}_{a_d} + \boldsymbol{K}_P(\boldsymbol{q}_{a_d} - \boldsymbol{q}_a) + \boldsymbol{K}_D(\dot{\boldsymbol{q}}_{a_d} - \dot{\boldsymbol{q}}_a)] \\ &- \boldsymbol{c}_a - \boldsymbol{g}_a - \boldsymbol{M}_{au}\boldsymbol{M}_{uu}^{-1}(\boldsymbol{c}_u + \boldsymbol{g}_u + \boldsymbol{s}_u.\end{aligned} \tag{2}$$

where the subscripts a and u refer to the actuated and unactuated parts of the dynamics, namely the UR10 robot and soft body, respectively. In the following, the term *complete PBFL* refers to (2). To assess how the soft body affects the motion of the UR10, a second simulation is performed with a FBL controller designed on the rigid part only, denoted as *incomplete PBFL*. Both control laws are implemented using the ID algorithm described in Pustina et al. (2025).

The control gains are $\boldsymbol{K}_P = 100 \cdot \boldsymbol{I}_6$ [Nm] and $\boldsymbol{K}_D = 50 \cdot \boldsymbol{I}_6$[Nms] and the initial configuration is

$$\boldsymbol{q}_0 = \begin{pmatrix} \mathbf{0}_{1\times 6} & \pi/4 & -\pi/4 & 0 \end{pmatrix}^T.$$

Fig. 6 reports the simulation results. When the complete PBFL is used, the configuration of the rigid robot converges exponentially fast to the reference, as expected. Instead, the incomplete PBFL has unsatisfactory performance, especially for the wrist joints, because the dynamic effects of the soft body are stronger at the end-effector. Nonetheless, the closed-loop is stable. In both cases, since the zero dynamics is asymptotically stable, the trajectory of the passive segment remains bounded. Initially, the motion requires a large control action because of the complete cancellation of the dynamics and the initial error.

1.7 Simulation 10: Regulation of PCC soft robot

This last simulation considers the shape regulation problem for a continuum soft robot with three bodies, modeled again under the PCC hypothesis. The base is rotated so that in the straight configuration the arm is aligned with the direction of the gravitational field. The kinematic and dynamic parameters are $L_{0_i} = 0.2$ [m], $R_i = 0.02$ [m], $\rho_i = 1070\,[\mathrm{kg/m^3}]$, $C_i = 5.55$ [GPa] and $\eta_i = 0.066$ [s]. The robot starts at rest from the straight configuration.

Despite oversimplifying the problem, we neglect the actuation model and assume the robot is fully actuated. Under these hypotheses, a simple PD with compensation of the potential forces fulfills the task, namely

$$\boldsymbol{\nu} = \boldsymbol{K}_P(\boldsymbol{q}_d - \boldsymbol{q}) - \boldsymbol{K}_D\dot{\boldsymbol{q}} + \boldsymbol{g}(\boldsymbol{q}_d) + \boldsymbol{s}(\boldsymbol{q}_d, \mathbf{0}_n), \tag{3}$$

where $\boldsymbol{q}_d \in \mathbb{R}^9$ is the desired (constant) reference. The control gains are set as $\boldsymbol{K}_P = 0.2$ [N m]([m]) and $\boldsymbol{K}_D = 0.1$ [N m s]([N s m^{-1}]), respectively. The reference consists of the following step commands, time spaced 5 [s] each,

$$\boldsymbol{q}_{d_1} = \begin{pmatrix} 1 & -1 & 0 & -1 & 0.5 & 0 & -1.5 & 0.8 & 0 \end{pmatrix}^T,$$
$$\boldsymbol{q}_{d_2} = \begin{pmatrix} -1 & 1 & 0 & 1 & -0.5 & 0 & 1.5 & -0.8 & 0 \end{pmatrix}^T,$$

and

$$\boldsymbol{q}_{d_3} = \begin{pmatrix} 0.5 & 0.5 & 0 & -0.3 & 0.3 & 0 & -1 & 1 & 0 \end{pmatrix}^T.$$

The above control law can be easily implemented using Algorithm 2 in Pustina et al. (2025). The only term depending on the model is the steady-state compensation of the potential forces, which can be computed with a single call to the procedure as $\boldsymbol{g}(\boldsymbol{q}_d) + \boldsymbol{s}(\boldsymbol{q}_d, \mathbf{0}_9) = \mathrm{ID}(\boldsymbol{q}_d, \mathbf{0}_9, \mathbf{0}_9)$. Fig. 7 reports the closed-loop results. As expected, the configuration variables quickly converge to the reference values. However, the robot oscillates during transients, as the stroboscopic plot shows.

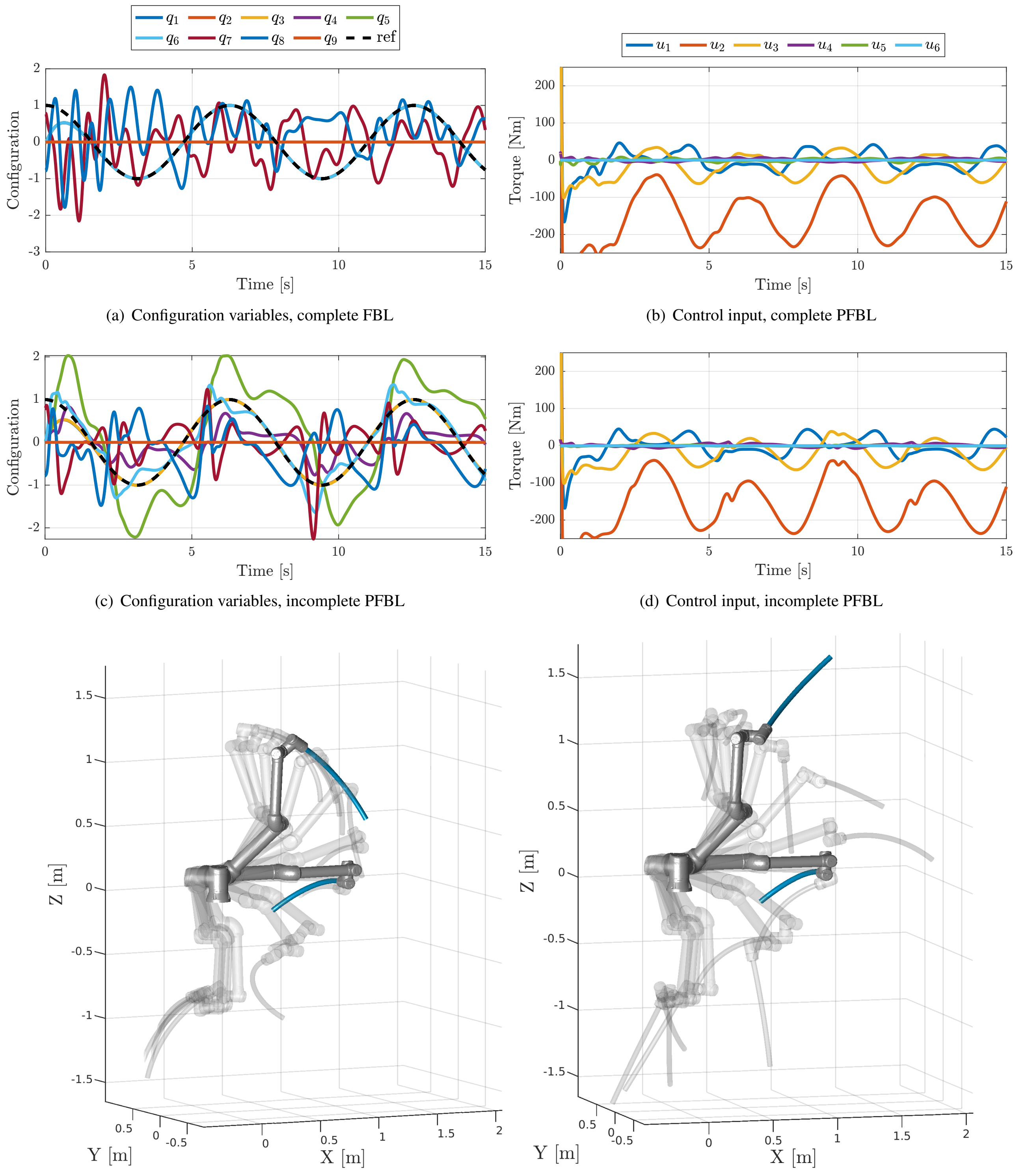

(a) Configuration variables, complete FBL

(b) Control input, complete PFBL

(c) Configuration variables, incomplete PFBL

(d) Control input, incomplete PFBL

(e) Stroboscopic plot, complete PFBL

(f) Stroboscopic plot, incomplete PFBL

Figure 6. Simulation 9: UR10 with PCC body. Time evolution of the (a) configuration variables (in $[\mathrm{rad}]$ and $[\mathrm{m}]$) and (b) control action under the complete PFBL controller (2) for a cosinusoidal reference. Similarly, (c)–(d) show the closed-loop performance under a FBL control law designed on the rigid part only. In (e)–(f), it is possible to see the robot motion for the two controllers.

References

Pustina P, Della Santina C and De Luca A (2025) Recursive model-agnostic inverse dynamics of serial soft-rigid robots. *Int. J. of Robotics Research* xx(yy): zz.

Renda F, Armanini C, Lebastard V, Candelier F and Boyer F (2020) A geometric variable-strain approach for static modeling of soft manipulators with tendon and fluidic actuation. *IEEE Robotics and Automation Lett.* 5(3): 4006–4013.

Renda F, Boyer F, Dias J and Seneviratne L (2018) Discrete Cosserat approach for multisection soft manipulator dynamics. *IEEE Trans. on Robotics* 34(6): 1518–1533.

Wang T, Halder U, Gribkova E, Gazzola M and Mehta PG (2022) Control-oriented modeling of bend propagation in an octopus arm. In: *Proc. American Control Conf.* pp. 1359–1366.

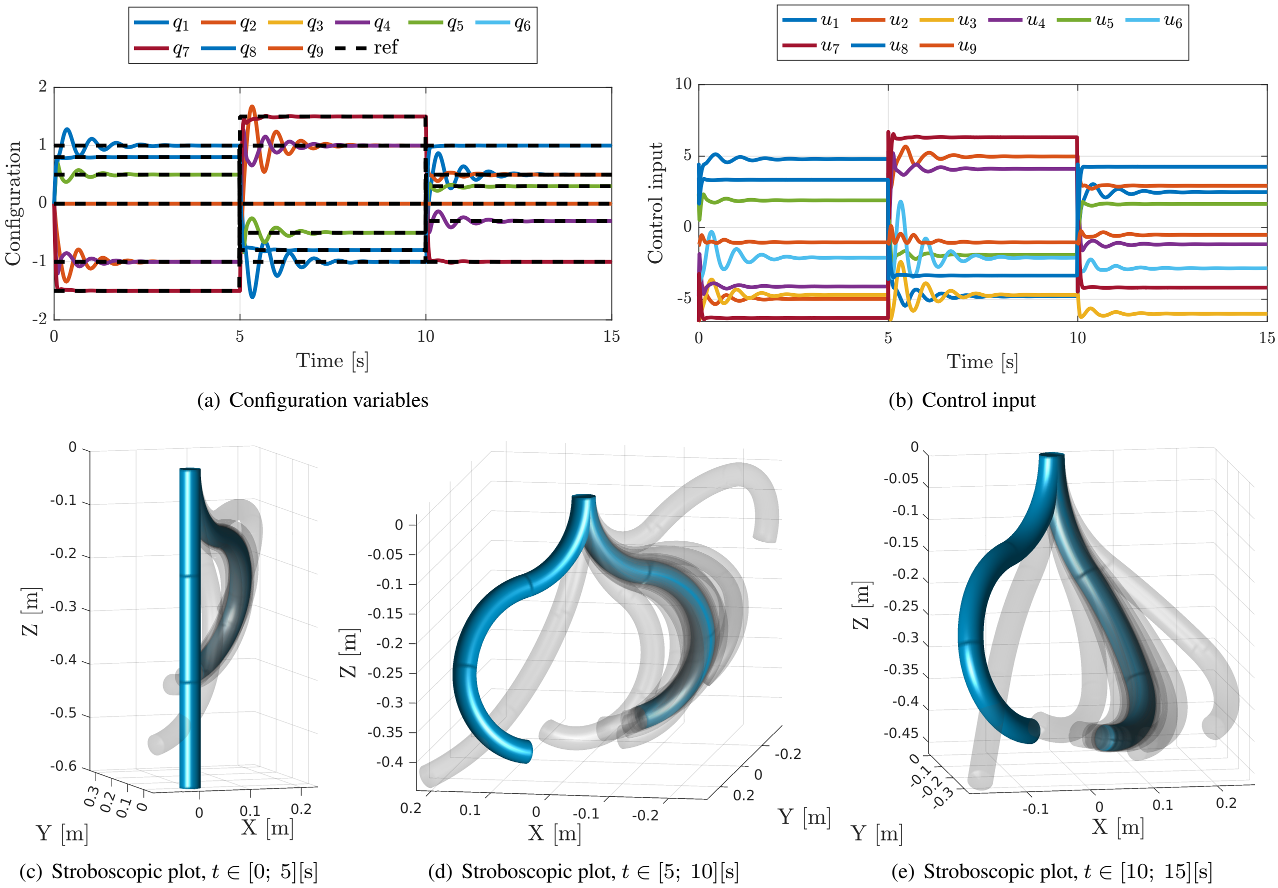

Figure 7. Simulation 10: Regulation of PCC soft robot. Time evolution of the (a) configuration variables (in $[\mathrm{rad}]$ and $[\mathrm{m}]$) and (b) control action (in $[\mathrm{N\,m}]$ and $[\mathrm{N}]$) under the PD+ regulator (3). Figs.(c)–(e) illustrate the robot motion in its workspace for the three references.